Energy-Based Stability Margin Computation Incorporating Effects of ULTCs

Madeleine Gibescu, *Member, IEEE*, Chen-Ching Liu, *Fellow, IEEE*, Hiroyuki Hashimoto, and Hisao Taoka, *Senior Member, IEEE*

***Abstract*—This paper introduces a new definition and computation method for the energy margin as a means to quantify the degree of stability of a dynamic power system model. The method is based on detailed device modeling that spans both transient and midterm time scales and includes effects of under-load tap-changer (ULTC) actions. The energy margin is defined as the minimum distance in potential energy space between the first- and second-kick trajectories, where the latter is chosen to be marginally stable. A generalized second-kick design is proposed. This consists of a combination of a load-step first kick and a three-phase fault second kick, applied at a time instant when the system is "closest" to the boundary of the stability region. The value of the energy margin is tracked through various tap-changer configurations. Thus, situations where ULTC actions are detrimental to stability can be uncovered, and "optimal" tap positions can be found. The concept is first illustrated on a single-machine infinite bus (SMIB); then, results are shown for a ten-bus voltage stability test system and for a modified version of the standard IEEJ 60-Hz test system, where some loads are fed through step-down ULTCs.**

***Index Terms*—Energy function, power systems dynamic stability, second-kick method, under-load tap changers (ULTCs).**

I. Introduction

In an operations planning environment, it is desirable to not only determine whether a set of dynamic disturbance scenarios are stable or unstable but also to assign a measure to their degree of stability, so various configurations can be compared and extrapolations made as to what transfer level would exhaust the available stability margin. Although transient and voltage stability—due to distinct mechanisms and separate time frames—have sometimes been perceived as decoupled phenomena, in this paper, they are treated as aspects of coupled short-term power system dynamics.

Various researchers have previously used energy function methods to quickly assess whether a transient disturbance will result in loss of stability; a classic text on the subject is [1]. Here, we do not focus on transient stability assessment methods that must yield results *fast* but rather on helping operations planners synthesize the output of simulations resulting in a multitude of time-domain curves into a single, easy-to-interpret number, namely, the energy margin (EM). A somewhat less general indicator of dynamic stability, called the extended equal area criterion (EEAC), has been developed in [2], based on clustering of multimachine systems to an equivalent single-machine infinite bus (SMIB). The EEAC has been successfully used for studies of transient stability constrained power systems, e.g., for contingency screening, corrective control, and available transfer capability (ATC) calculations [3].

Significant research has been devoted to the dynamic aspects of voltage stability. A saddle-node bifurcation analysis has been applied to voltage collapse in [4] and [5], where dynamic generator and load models are used. Reference [6] takes a time decomposition approach for detecting voltage stability problems, in which a simulation tool for midterm dynamics provides system "snapshots" to be used in an eigenvalue analysis of the faster, transient dynamics. A few papers have been devoted to advancing energy function methods for the study of voltage stability. An energy function that incorporated load modeling but no generator dynamics was first introduced in [7], while an energy function that takes into account reactive power limits is proposed in [8]. Finally, a Lyapunov function for structure-preserving power system models with both generator and load dynamics is developed in [9].

In this paper, an energy function formulation is developed from the first-integral approach, using injection models. Our time-domain simulations use detailed models for generators, exciters, governors, dynamic loads, and under-load tap-changer (ULTC) devices; hence, the proposed method can be as accurate as the system model allows. Based on the trajectories obtained, an energy value is calculated for every point in time. The energy margin is then constructed based on the established second-kick method, as the potential energy (PE) difference at the respective peaks of the first- and second-kick disturbances. Since we are not restricted in our assessment by the transient stability time frame, we are able to introduce a new, "generalized" EM concept, where more freedom is allowed in the choice of the nature of both the first and second kicks and also in the timing of the second-kick application. The only requirements are that 1) the first- and second-kick trajectories settle in the *same* stable equilibrium point (SEP) and that 2) the second-kick trajectory is *marginally* stable, i.e., it passes as close as possible to an unstable equilibrium point (UEP) on the boundary of the stability

Manuscript received October 28, 2003; revised October 5, 2004. This work was supported in part by the Advanced Power Technologies (APT) Center at the University of Washington. The APT Center is sponsored by AREVA T&D, BPA, CESI, LG Industrial Systems, Mitsubishi Electric, PJM Interconnection, and RTE France. Paper no. TPWRS-00604-2003.

M. Gibescu is with the Power Systems Laboratory, Delft University of Technology, 2600 GA Delft, The Netherlands (e-mail: m.gibescu@ewi.tudelft.nl).

C.-C. Liu is with the Department of Electrical Engineering, University of Washington, Seattle, WA 98195-2500 USA (e-mail: liu@ee.washington.edu).

H. Hashimoto is with the System Optimization Technology Department, Advanced Technology R&D Center, Mitsubishi Electric Corp., Amagasaki, Hyogo 661-8661, Japan (e-mail: Hashimoto.Hiroyuki@wrc.melco.co.jp).

H. Taoka is with the Department of Electrical and Electronic Engineering, Fukui University of Technology, Fukui 910-8505, Japan (e-mail: taoka@ccmails.fukui-ut.ac.jp).

Digital Object Identifier 10.1109/TPWRS.2005.846053

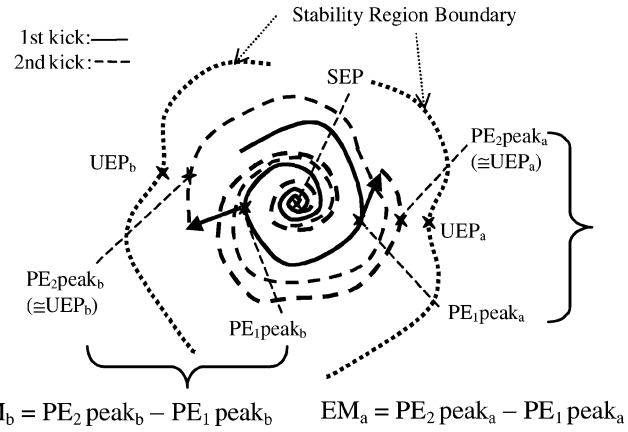

Fig. 1. Second-kick-based energy margin computations.

region while still remaining within the region of attraction of the aforementioned SEP.

In transient stability assessment, the first- and second-kick disturbances are three-phase faults of specified duration at the same location in the system. In this paper, a new second-kick design is proposed. It consists of a combination of load step first kick and three-phase fault second kick, applied in the region that experiences the load increase. The idea is to first bring the high (stable) and low (unstable) voltage solutions closer together at this higher load level, then to drive the system toward the stability boundary via a fault. Other first-second kick combinations that meet conditions 1 and 2 above could be explored, such as a permanent load step as first-kick followed by temporary load step as second-kick or permanent fault (with line clearing) followed by temporary load step.

It is observed that the first-kick trajectory results in a potential energy curve that exhibits multiple local peaks. Applying the second kick at time instances corresponding to these PE peaks may drive the system toward different UEPs, thus uncovering different margins for different types of instability mechanisms. This is illustrated in Fig. 1, which shows as a continuous line the original first-kick trajectory settling at an SEP. This stable trajectory is situated within the SEP's stability region, whose boundary is shown in a dotted line. Two marginally stable second-kick trajectories a and b are shown in dashed lines, the first one originating at a peak point of the first-kick PE, marked as $\mathrm{PE}_1\mathrm{peak}_\mathrm{a}$, and the second one at $\mathrm{PE}_1\mathrm{peak}_\mathrm{b}$. Each of these trajectories has its own controlling UEP, UEP_a, and UEP_b, both situated on the boundary of the stability region. Approximations to these UEPs are taken as the PE peaks of the second-kick trajectories, $\mathrm{PE}_2\mathrm{peak}_\mathrm{a}$ and $\mathrm{PE}_2\mathrm{peak}_\mathrm{b}$, respectively. Subtracting the values of the second- and first-kick PE peaks results in two values for the energy margin, EM_a and EM_b, and the smallest will be taken as the actual margin. Thus, the margin calculated at various PE peak times can be smaller or larger, as the stability region boundary can be shaped such that the system is closer to instability in one particular direction.

For certain power system models that result in steady-state equilibria for which the boundary of the stability region is characterized not by UEPs but by an unstable limit cycle (ULC), as illustrated, for instance, in [10], the search for a marginally stable trajectory will encounter a system response that exhibits sustained oscillations. Trajectories originating outside the limit cycle diverge away via growing oscillations, while trajectories inside the limit cycle converge to the SEP via decreasing oscillations. Since the limit cycle is a closed curve, the energy along such a trajectory would be bounded and periodic. In such a case, the marginally stable trajectory originating inside the limit cycle can be used in computing the EM. In addition, a special case of limit cycles for mixed continuous and discrete dynamics may arise from switching events. Note that the transformer tap hunting phenomenon is excluded from this analysis, as we make the assumption that the number of tap-changing operations has to be finite.

Our previous work [11] has shown that the energy margin and UEP coordinates are dependent on the site, timing, and nature of the disturbance and, of course, on the initial power flow solution. We have proposed using the EM for making decisions about installing stability-enhancing devices such as SVCs and TCSCs. Higher margins were indeed reported for systems equipped with these devices. In addition, different values for the energy margin were reported for the traditional and new second-kick designs, thus reflecting different instability mechanisms.

This paper offers a principled approach to investigate the effects of transformer tap-changer actions on system stability. The interactions between loads, generators, and ULTCs are all accounted for, and longer simulation times than those typically involved in the assessment of transient stability are used. A new energy-based tool for the analysis of short-term power system stability, with transformer tap ratios modeled as time-changing parameters, has been devised. Energy margins are calculated for the newly designed second kick as the system evolves through various tap-changer configurations. The individual EM values are not an indication of the degree of long-term voltage stability, as each EM corresponds to a fixed tap ratio; however, the overall trend should provide some guidelines for desirable ULTC settings.

The second-kick-based EM computation method described in our previous work [11] is extended to allow for dealing with systems equipped with ULTCs. This paper starts with an SMIB example, which serves to illustrate that, for such a simplified model, the ULTC acts—as intuitively expected—to improve the system stability as measured by the EM. Results are then shown for a simple ten-bus voltage stability test system [12] and finally for a modified version of the standard IEEJ 60-Hz test system analyzed in [11], with select loads now fed through step-down ULTC transformers. In the scenario shown for the ten-bus system, contrary to expectations, EM decreases with the tap-changer action. This is explained by the effect of a generator over-excitation limiter (OXL) that curtails reactive power supply from generation nearby the load center, similar to the voltage collapse mechanisms reported, e.g., in [13]. The IEEJ 60-Hz system is used to illustrate how the EM concept and computation algorithm can be applied to a large, realistic, multimachine and multi-ULTC case. The results shown for this system scenario reveal the existence of an "optimal" tap configuration, as the EM initially increases due to improvements in the voltage profile and load damping, then starts to decline as the voltage-dependent real loads are gradually restored via their step-down ULTC transformer actions.

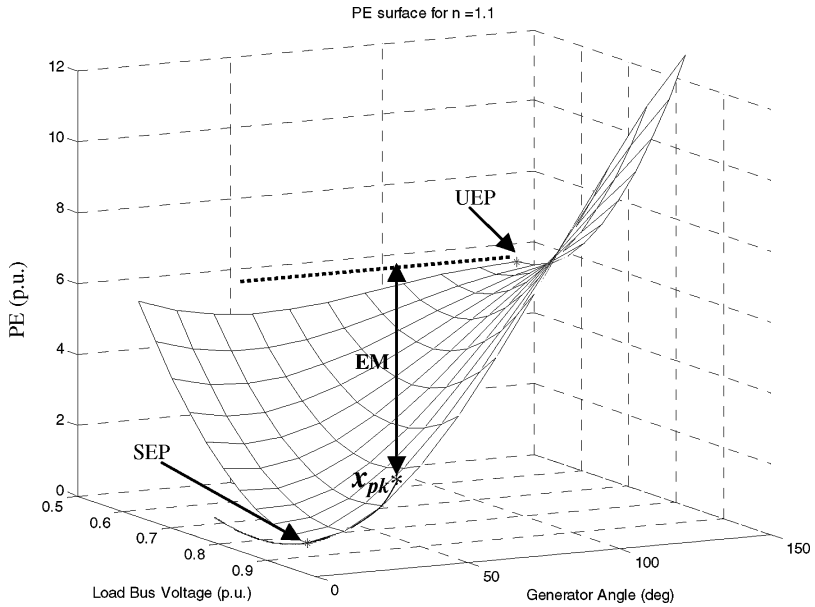

Fig. 2. Potential energy surface for SMIB at tap ratio 1.1.

II. Simple Example: SMIB With ULTC

To illustrate the concept of EM computation in the presence of ULTCs, a simple power system adapted from [14], consisting of a load connected to both a generator and an infinite bus in a triangle configuration, has been extended to allow for the modeling of a step-down transformer at the load bus. The generator is modeled via the constant voltage behind transient reactance model, while the load is constant MVA. This simplified modeling, although not appropriate for the study of voltage stability, allows for the definition of a path-independent energy function. Then, the energy margin can be defined as the minimum height of the potential energy (PE) "well," i.e., the difference between the energy of the UEP and the energy of the PE peak point along the trajectory x_{pk}, as illustrated in Fig. 2. This height is proportional to the energy of the unstable equilibrium point (UEP) responsible for transient instability, whose coordinates can, in this case, be explicitly calculated for each tap ratio value.

Simulations show that for this simple model, the energy of the transient UEP increases, while the ULTC acts to restore the load bus voltage by decreasing the tap ratio. The transient UEP does remain the controlling UEP for the whole ULTC turns ratio range. In addition, the energy of the critical point decreases with each subsequent tap action, and so, it follows that the energy margin is improved. Fig. 3 shows the kinetic (KE), potential (PE), and total (W) energy trajectories as the system evolves through three tap positions, of ratio 1.1, 1.0, and 0.9 respectively. The PE peak point of each region is identified, and the energy margins (EMs) are calculated as the difference between the energy of the UEP for that tap position and the energy of the respective peak point $\mathrm{PE}_{\mathrm{peak}}$.

Our simulations also indicate that the tap-changer action results in increased reactive power support from the classical generator, which, per its definition, does not contain any reactive power limiting mechanisms. More interesting results will be shown when this simplifying assumption is no longer made.

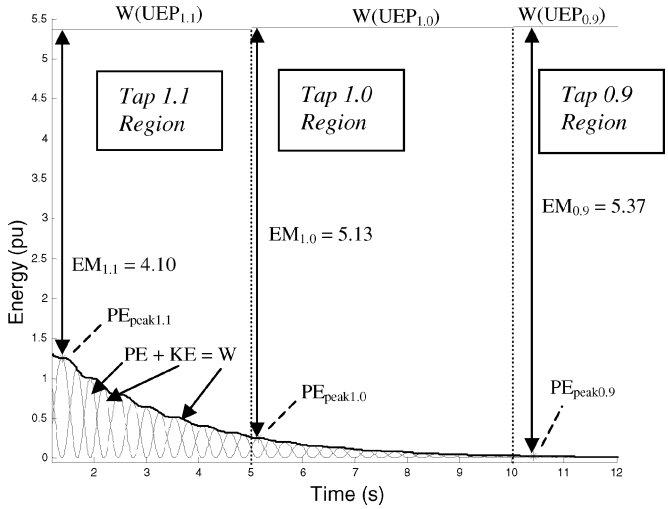

Fig. 3. Energy trajectory and margin versus time for SMIB with ULTC.

III. Methodology

A. Energy Function Formulation

Starting from the basic idea of the first integral approach, as in [15] and [16], i.e., that the right-hand sides of the nonlinear ordinary differential equations (ODEs) that make up the dynamic power system model can be viewed as negative partial derivatives of the energy function W with respect to the states

$$T \cdot \dot{x} = h(x) = -\frac{\partial W}{\partial x} \tag{1}$$

it can then be shown that the energy W that satisfies (1) will be decreasing along any system trajectory, i.e., $\dot{W} \leq 0$, and that the set of points for which $\dot{W} = 0$ contains only equilibria.

The energy function is traditionally comprised of two terms: potential and kinetic energy

$$W(x,t) = W_{\mathrm{PE}} + W_{\mathrm{KE}}. \tag{2}$$

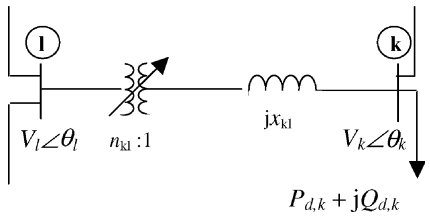

Fig. 4. ULTC transformer branch connected to load.

The kinetic energy is simply

$$W_{\mathrm{KE}}=\frac{1}{2}\sum_{i\in G}M_i\omega_i^2 \tag{3}$$

while the potential energy derived from time-domain simulated trajectories has been originally developed in [11] as

$$\begin{aligned}W_{\mathrm{PE}}&=\left[-\frac{1}{2}\sum_{i\in L\cup G}V_i^2B_{ii}-\frac{1}{2}\sum_{i\in L\cup G}\sum_{j\neq i}V_iV_jB_{ij}\cos(\theta_i-\theta_j)\right]\Bigg|_{(V^s,\theta^s)}^{(V,\theta)}\\&\quad-\sum_{i\in G}\int_{\delta_i^s}^{\delta_i(t)}(P_{mi}-P_{ei})d\delta_i+\sum_{i\in L\cup G}\int_{t^s}^{t}P_i(t)\dot{\theta}_i dt\\&\quad+\sum_{i\in L\cup G}\int_{t^s}^{t}\frac{Q_i(t)}{V_i}\dot{V}_i dt\end{aligned} \tag{4}$$

where

- superscript s denotes the steady-state equilibrium point;
- δ and ω are the relative machine internal angle and speed;
- P_m and P_e are machine mechanical and electrical powers;
- B_{ii} and B_{ij} are the imaginary parts of the bus admittance matrix (under the lossless model assumption);
- $V\angle\theta$ are magnitude and angle of the complex bus voltages;
- P and Q are injections at the load (L) and generator (G) terminal buses.

For the detailed machine and load modeling used in this paper, the integral terms in the expression of the potential energy (4) are path dependent. However, since the whole time-domain curves are available through simulation, including the final SEP, these terms can be computed accurately. A numerical method similar to [17] and [18], e.g., the backward trapezoidal integration method, can be used to calculate the energy function incrementally for every point in time along the simulated trajectory.

B. Variation of UEP Energy With Respect to Tap Ratio

Let us consider a lossless, multimachine differential-algebraic equation (DAE) power system model, which allows for the definition of a path-independent energy function. Now, let us examine the effect of introducing a ULTC transformer at branch k–l, as illustrated in Fig. 4. The following terms in the expression for potential energy (4) will be explicitly dependent on the tap ratio:

$$\begin{aligned}W_{\mathrm{PE}}&=\ldots\left[-\frac{1}{2}V_kV_l\frac{b_{kl}}{n_{kl}}\cos(\theta_k-\theta_l)\right.\\&\quad\left.-\frac{1}{2}V_lV_k\frac{b_{lk}}{n_{kl}}\cos(\theta_l-\theta_k)-\frac{1}{2}\left(-\frac{b_{kl}}{n_{kl}^2}\right)V_l^2\right]\Bigg|_{x^s}^{x}\end{aligned} \tag{5}$$

where $b_{kl}=1/x_{kl}$ is susceptance of the k–l transformer branch.

It is necessary to determine how the energy of the UEP changes with respect to the transformer tap ratio n, where, for the purposes of this proof, n is treated as a continuously varying parameter. The derivative of the energy function with respect to the tap ratio can be written as

$$\frac{dW}{dn}=\frac{\partial W}{\partial n}+\frac{\partial W}{\partial x}\cdot\frac{\partial x}{\partial n}+\frac{\partial W}{\partial y}\cdot\frac{\partial y}{\partial n}$$

where

$$x=[\,\delta\quad\omega\,],\ y=[\,V\quad\theta\,]. \tag{6}$$

It is noted that, since the energy function reaches a maximum at the UEP, the partial derivatives of the energy W with respect to the differential and algebraic variable vectors x and y calculated at the UEP must be zero. Hence

$$\left.\frac{dW}{dn_{kl}}\right|_{x^u}=\left.\frac{\partial W_{PE}}{\partial n_{kl}}\right|_{x^u}=\left.\frac{\alpha\cdot n_{kl}-\beta}{n_{kl}^3}\right|_{x^s}^{x^u} \tag{7}$$

where $\alpha=V_kV_lb_{kl}\cos\theta_{kl}$ and $\beta=V_l^2b_{kl}>0$.

Note that β is always positive, whereas the sign of α can be either positive or negative, depending on the value of $\cos\theta_{kl}$:

$$\cos\theta_{kl}<0,\ \text{i.e.}\ |\theta_{kl}|>\frac{\pi}{2}\Rightarrow\alpha<0. \tag{8}$$

For negative values of α, the numerator in (7) will be clearly negative. For positive values of α, the numerator in (7) is cancelled with respect to n_{kl} at

$$n_{kl}{}^*=\frac{\beta}{\alpha}=\frac{V_l}{V_k\cos\theta_{lk}}>1.0. \tag{9}$$

However, within the usual range of operation of transformer tap changers, which is $0.90\ldots1.10$ turns ratio, the numerator in (7) typically stays negative even for positive values of α. Thus, the derivative of the UEP energy can be viewed as the difference between two negative functions of the type in (7), one dependent on the UEP coordinates and another on the SEP coordinates. The energy of the UEP can then be viewed as the difference between two functions decreasing with respect to a tap-ratio increase. Depending on the actual SEP and UEP coordinates, the result of this difference can be an increasing and/or a decreasing function. From this theoretical assessment, one can conclude that even when the controlling UEP is consistent throughout the various tap-changer configurations, the energy of this UEP can either go up, resulting in a higher potential energy well and, consequently, a more stable configuration, or down, when quite the opposite is achieved. The following section will describe a rigorous method by which the stability of a system equipped with

discrete tap-changing transformers can be tracked through its various configurations.

C. Second-Kick Energy Margin for Discontinuous Systems

A unified approach, covering short-term voltage and angle instability mechanisms, is proposed in this paper. This is based on the fact that the loss of stability is always preceded by the system trajectory leaving the region of attraction of the post-fault stable equilibrium point, through a boundary point in the "vicinity" of a UEP. The stability boundary can be locally approximated by the constant potential energy surface passing through this UEP. Traditionally, the energy margin is defined as the difference between the energy injected into the system by the fault (i.e., at fault clearing) and the energy of the UEP, provided that its coordinates are known [19]. The second-kick method allows one to avoid the computational burden imposed by the need to determine the UEP by naturally providing a good approximation of the controlling UEP, i.e., the one toward which the unstable trajectory would be headed. The method takes advantage of the modeling accuracy of time-domain simulations and can deal with path-dependent energy functions without the need for making unrealistic modeling simplifications.

As mentioned in the introduction, in order for the "margin" concept to make sense, one must be able to guarantee that the system converges to the same steady-state equilibrium point after both the first and the second kick. Only under such conditions can one talk about the distance in the potential energy space between these two trajectories. Since the power flow solution is different for every region of constant tap configuration, it is necessary to calculate a new EM for each of these regions with the tap configuration identical in the first and second kick. The algorithm below is a modified version of the EM computation algorithm we first employed for systems with a continuous model [11].

- Simulate the original first-kick system trajectory with ULTC model enabled: $x(t)$.
- Divide the trajectory into regions of constant tap configuration: $x_1(t) \ldots x_{\mathrm{n}}(t)$, and save their initial conditions: $x_{01} \ldots x_{0\mathrm{n}}$.
- Starting from initial condition x_{0k}, generate new first-kick trajectories $x'_k(t)$, with ULTCs locked in the kth tap position set $k = 1 \ldots n$.
- Apply the second-kick method for each of the above continuous trajectory regions $x'_k(t)$, with ULTCs locked, i.e., at chosen time t'_k, initiate disturbance that results in a marginally stable trajectory.
- Compute set $\{\mathrm{EM}_1 \ldots \mathrm{EM}_{\mathrm{n}}\}$ of energy margin values for the system locked in each tap configuration.

For each constant tap configuration region k, the energy margin is calculated as

$$\mathrm{EM}_k = \int_{t_{ss,k}}^{t''_k} \frac{dPE_{k,2}}{d\tau} d\tau - \int_{t_{ss,k}}^{t'_k} \frac{dPE_{k,1}}{d\tau} d\tau \qquad (10)$$

where $t_{ss,k}$ is the time the post-fault steady-state equilibrium is reached, t'_k is the time instance when the second kick is applied (chosen from peak times of PE terms in the first-kick trajectory), and t''_k is the PE peak time of the second-kick trajectory.

This algorithm has been implemented via a *Perl-C-Matlab* hybrid and tested on two power systems featuring discrete ULTC models, as shown in the results section below.

IV. Results

In a dynamic security assessment (DSA) study, many disturbance scenarios, at various locations in the system, must be simulated. This is also done in traditional transient stability studies, with an energy margin or some other index, such as the one derived from the EEAC, assigned to each scenario. In this paper, instead of a single number per scenario, a set of numbers, one for each continuous region in between discrete switching events, is calculated. Since each EM value corresponds to a fixed tap configuration, the one that exhibits the maximum value of the EM as obtained in a study environment can be used as a guide to suggest tap settings for ULTCs during real-time operation. Eigenvector- or tangent-vector-based network partitioning techniques [20] can be applied to identify areas that are vulnerable to voltage collapse. Buses within such areas can be then be used as locations for the first-kick load step, such as load centers located remotely from generation sources. Further, the three-phase fault should be applied in the area of the transmission system supplying power to such a load, to decrease the transfer capability. The results section focuses on nearly radial structures, as it is generally agreed that such systems are more vulnerable to voltage stability than meshed networks, where reactive power is more readily available from nearby sources without extensive losses.

A. Ten-Bus Voltage Stability Test System

The EM with ULTC computation method has been applied to a modified version of the ten-bus voltage-stability test system described in [12]. The one-line diagram is shown in Fig. 5.

This system consists of the following dynamic models.

- G1 is a classical machine with large inertia and MVA; fast-responding governor, to approximate an infinite bus.
- G2 and G3 have subtransient models with fast exciters.
- The excitation for G3, which is on the same side as the load center, is modeled in detail with an OXL that limits its ability to supply reactive power.
- Transformer T6 is equipped with an ULTC, turns ratio range $0.90 \ldots 1.10$, 0.00625 step size, 30.0 s. time delay for first tap move and 5.0 s. for second and subsequent moves.

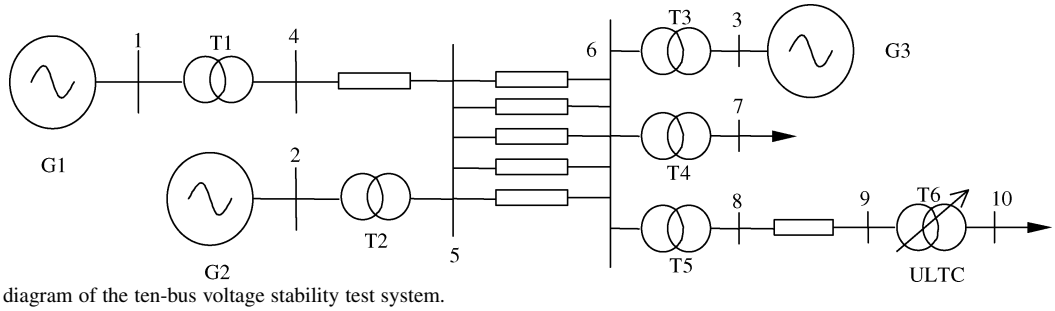

Fig. 5. One-line diagram of the ten-bus voltage stability test system.

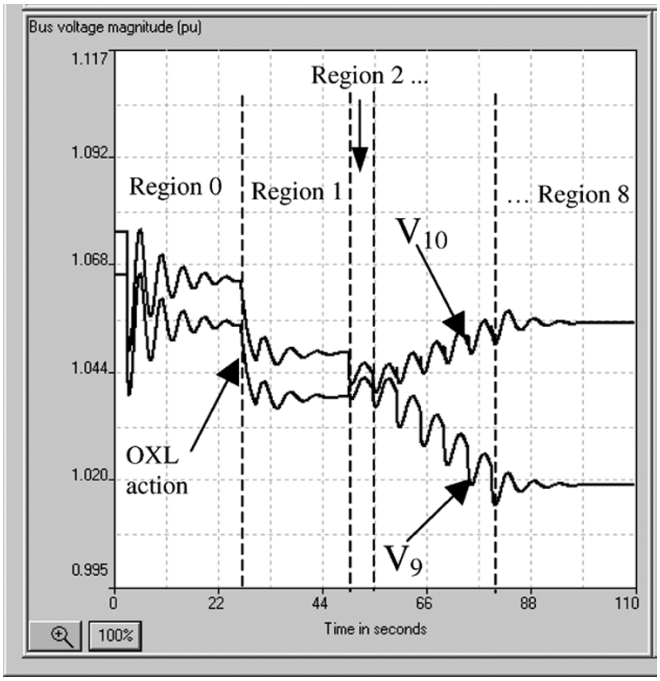

Fig. 6. Bus voltage magnitudes at primary and secondary sides of the ULTC.

- Megawatt loads at buses 7 and 10 are 100% V-f dependent; MVAr loads are 50% constant Z and 50% constant I.

The original disturbance, a.k.a., first kick applied, was chosen as a permanent 2% load step at both load buses, 7 and 10. After an initial voltage decrease, which is further aggravated at about 30 s by the limiting action of the OXL at G3, the ULTC kicks into action at about 50 s. After seven tap changes, the voltage at load bus 10 is restored, although to a value somewhat lower than in its prefault steady state.

The time-domain trajectory was divided into nine regions, as shown in Fig. 6, with Region 0 and 1 prior to any tap-changing action and Regions 2–8 corresponding to the time intervals between two consecutive tap actions. The oscillations in between tap changes are due to the voltage restoration effect of the ULTC, followed by the voltage decrease effect of load restoration [12]. The EM calculations were then carried out for Region 0 prior to any OXL action, Region 1 after OXL but with the ULTC action disabled completely, Region 2 with the ULTC locked after the first tap move, and so on, until Region 8 with the ULTC locked after the seventh (last) tap move.

The second-kick disturbance was a temporary three-phase fault applied at bus 6, followed by the opening of one of the circuits of line 5–6, with reclosing after fault clearing. The second kick was applied for each region at the PE peaks of the original trajectories, following their respective tap-changing action, as described in Table I.

TABLE I
SECOND-KICK EM RESULTS, TEN-BUS VOLTAGE STABILITY TEST SYSTEM

Reg. no.	Switching action (s)	EM (p.u.)	EM (%)	P (MW)	Q (MVAr)	S (MVA)
0	-- (pre-OXL)	4.193	100.0	6602	3278	7371
1	OXL @ 30.15	3.323	79.3	6771	3262	7516
2	1st tap @ 49.75	3.237	77.2	6770	3299	7531
3	2nd tap @54.79	3.219	76.8	6768	3338	7546
4	3rd tap @59.84	3.170	75.6	6766	3376	7561
5	4th tap @64.88	3.114	74.3	6763	3416	7577
6	5th tap @69.93	3.061	73.0	6760	3456	7592
7	6th tap @74.97	2.997	71.5	6757	3496	7608
8	7th tap @ 79.97	2.993	71.4	6754	3537	7624

From Table I, one can see that for this particular system model and disturbance type, the energy margin is decreasing with each tap action. In an attempt to explain this counterintuitive result, one can look at the evolution of the system generation and load due to the ULTC. The first thing to note is that by the time the ULTC control mechanism is activated, the OXL at G3 has already intervened to curtail the reactive support from this generator, which is closest to the load center. As the tap-changing actions restore the voltage at load bus 10, the voltage at load bus 7 is actually decreasing. The overall effect of this increase/decrease is that both the system real and reactive loads are actually slightly decreasing with each tap action. However, due to the restoration of the voltage at bus 10 by the ULTC action, the local reactive support from G3 is less with each tap action, while support from G1 and G2 must correspondingly increase, as seen in Fig. 7. Since the extra MVArs must come from sources more distant from the load center, losses are increased, hence the extra stress on the system.

The system MVA generation at the final steady-state point of each tap region is also summarized in Table I—note that total MVA is increasing with each tap position. Fig. 8 shows the plot of energy margin values versus system MVA generation for each trajectory region. Note that the largest change in EM happens due to the OXL action, after which EM continues to slowly decrease with each tap position change.

B. IEEJ 60-Hz Multimachine With Multi-ULTC Test System

The IEEJ 60-Hz test system is a radial system with 27 buses, 35 branches, and ten machines [11].

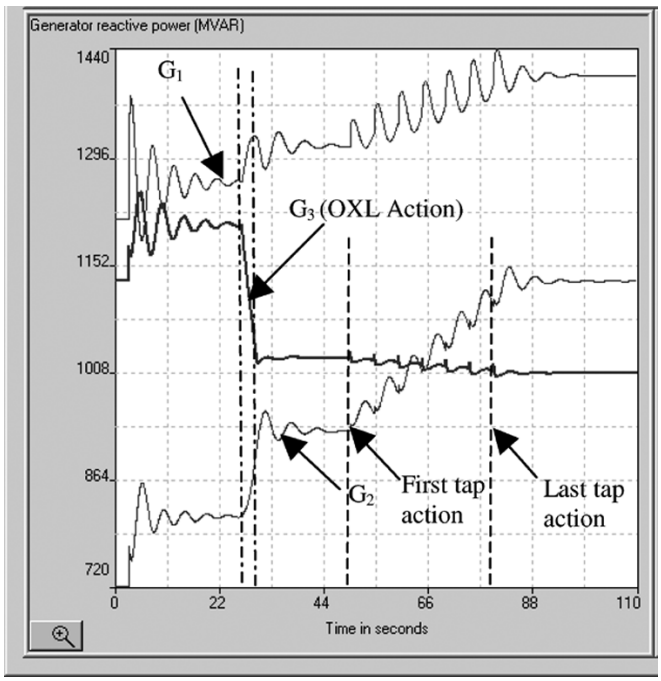

Fig. 7. Generator reactive power, original 2% load step, and ULTC action.

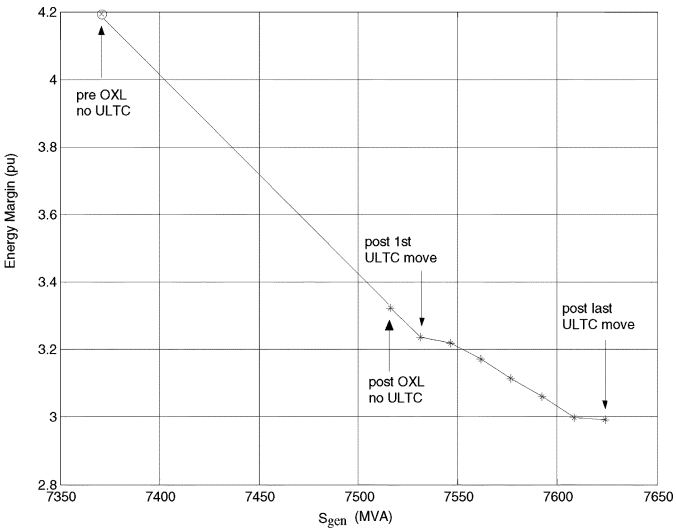

Fig. 8. Energy margin versus system MVA generation for each tap position.

The one-line diagram is shown in Fig. 9. Loads at buses 2–8 have been modified to be fed through step-down ULTCs. This system consists of the following dynamic models.

- Generators are modeled by the detailed two-axis subtransient model with exciter and governor.
- Real power load is voltage and frequency dependent, as shown in (11); reactive power load is constant impedance.
- ULTCs turn ratio range $0.95\ldots1.05$, 0.005 step size, 6.0 s time delay between moves.

The real power load model used is

$$P(V,f) = \left(\frac{P}{V}\right)_{ss} V(1 + k_{pf}\Delta f) \tag{11}$$

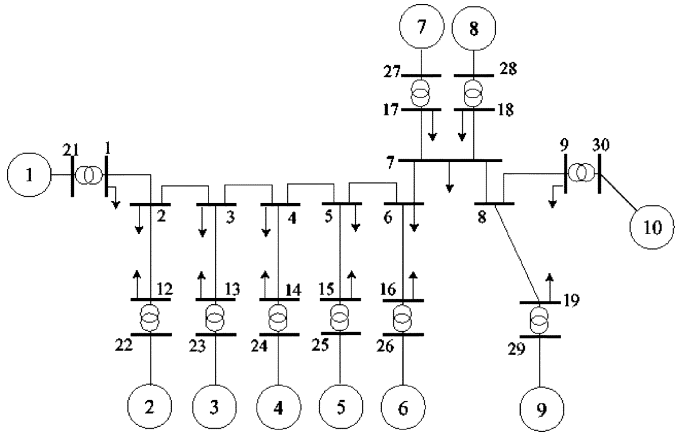

Fig. 9. One-line diagram of the IEEJ 60-Hz test system.

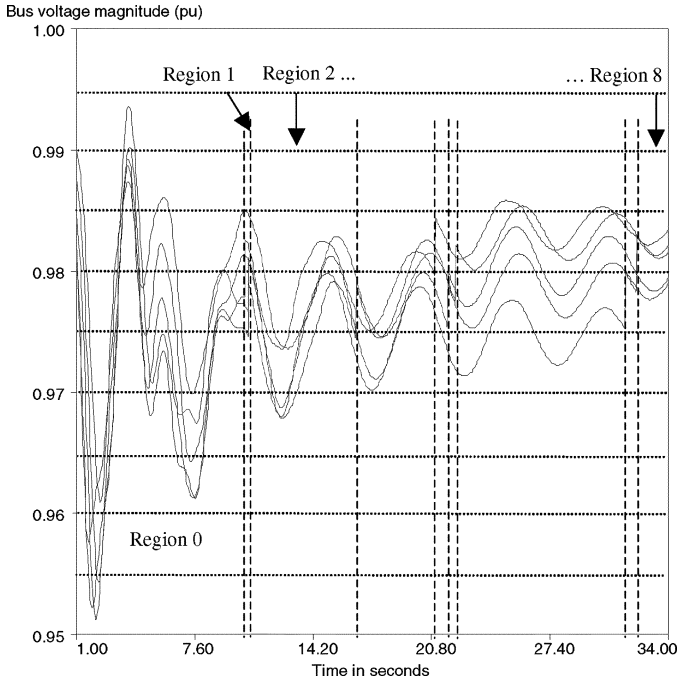

Fig. 10. Load voltage profile for the modified IEEJ 60-Hz system.

where superscript ss denotes prefault steady-state values, k_{pf} is a constant positive coefficient, and Δf represents the frequency deviation from nominal (60 Hz).

With the energy function defined as in (2)–(4) and the load model as in (11), it can be shown that the derivative with respect to time of the energy function is negative definite

$$\dot{W} = -\sum_{i\in G} D_i\omega_i^2 - \sum_{i\in L}\left(\frac{P_i}{V_i}\right)_{ss} V\cdot k_{pf}\left(\frac{\dot{\theta}_i}{2\pi}\right)^2 \le 0 \tag{12}$$

where D_i is the generator damping coefficients, and $\dot{\theta}_i$ is the rate of change of load bus angles.

In order to evaluate the degree of stability of this system through the EM, a first kick consisting of a 10% load increase at buses 6 and 9 is applied, for a total of 80 s simulation time until steady state is achieved. This disturbance results in nine constant tap regions, with the first tap action occurring at about 10 s into the first-kick simulation and the last one at about 32 s, as illustrated in Fig. 10.

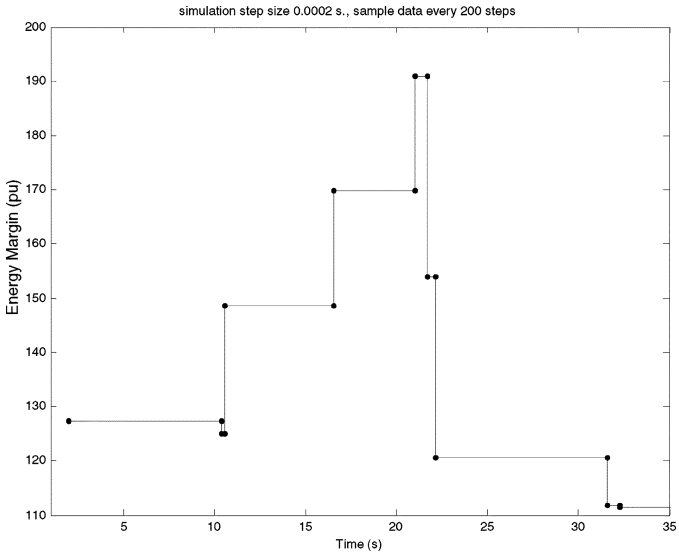

Fig. 11. Energy margin versus time for the modified IEEJ 60-Hz system.

TABLE II
SECOND KICK EM RESULTS, IEEJ 60-HZ TEST SYSTEM

Reg. no.	Tap change time (s), Bus#	EM (p.u.)	EM (%)	P (MW)	Q (MVAr)	S (MVA)
0	-- (pre-ULTC)	127.7	66.86	110025	38310	116504
1	10.40, Bus 6	125.2	65.60	110041	38321	116523
2	10.59, Bus 7+8	148.7	77.85	110074	38364	116568
3	16.59, Bus 5	170.0	89.00	110090	38366	116584
4	21.03, Bus 8	191.0	100.0	110102	38388	116602
5	21.72, Bus 6	153.9	80.58	110119	38392	116620
6	22.17, Bus 4	120.7	63.20	110136	38397	116637
7	31.61, Bus 7	111.8	58.53	110157	38416	116663
8	32.26, Bus 5	111.5	58.38	110174	38418	116680

The second kick chosen was a three-phase fault at bus 16, which is the high-voltage side of a generator step-up transformer and within the first-tier neighborhood of stressed load bus 6. The minimum EM value obtained for each tap configuration region is shown in Fig. 11.

The time-domain simulation engine used was the transient stability assessment tool (TSAT) from Powertech Labs [21].

Following a negligible decrease due to the first tap position change, the EM increases to its maximum value at about 20 s post-disturbance, then decreases to a final value slightly lower than the one before any tap action occurred. The dynamic behavior for this large multi-ULTC system is more complex than that of the single-ULTC ten-bus system examined in the previous section. Still, there is a plausible explanation for the results in Fig. 11 based on the properties of voltage- and frequency-dependent loads. Table II shows the values of the EM for each constant tap-configuration region along the first-kick trajectory, together with post-fault steady-state values of system generation.

One can notice from this table that, due to the voltage and, hence, load restoration effects of ULTCs, the system MVA increases steadily with each tap action. This should, by a similar argument as in the previous section, lead to an ever-decreasing energy margin. However, the voltage restoration has a secondary effect, which is that it linearly improves the load-damping coefficient $k_{pf} \cdot V$ in front of the frequency-deviation Δf in the load model (11). A better damped system is able to absorb larger amounts of energy as injected by the fault and still remain stable. This is also reflected in the expression of the energy function derivative (12), which is larger for higher load damping and, thus, results in a faster decreasing energy function curve. By itself, this effect would result in an increasing energy margin.

Due to the above two competing effects, the EM increases for the first couple of tap changes, as the voltage profile is improved and the system becomes better damped, after which the higher loading on the system becomes the dominant effect, and the EM starts to decrease for the last four tap changes. The load behavior ties together the voltage response—as governed by ULTCs—and the frequency response—as governed by generators.

We believe that this research shows the potential for using the proposed EM with ULTC computation algorithm for offline studies that would allow operations planners to visualize the impact of various tap-changer configurations on system stability.

V. CONCLUSION

This work has shown that the energy margin can be used as an indicator of the degree of stability of power systems with ULTCs, thus aiding operators and planners in making decisions about the most suitable tap-changer configurations and uncovering situations where tap actions can actually be detrimental to system stability.

The energy function proposed featured detailed modeling of generators, dynamic loads, and ULTCs. No approximations were made since complete information regarding the system response to a disturbance is available via the time-domain simulation. The tradeoff is that this method is very time consuming and as yet only suitable for offline studies. However, a fully automated tool that computes the energy margin for each tap-changer configuration resulting from a chosen first-kick disturbance has been devised and tested on a realistic multimachine, multi-ULTC system.

ACKNOWLEDGMENT

The authors would like to thank L. Wang and F. Howell of Powertech Labs, British Columbia, Canada, for their assistance with modeling and simulation issues in TSAT.

REFERENCES

[1] A. A. Fouad and V. Vittal, *Power System Transient Stability Analysis: Using the Transient Energy Function Method.* Englewood Cliffs, NJ: Prentice-Hall, 1991.

[2] Y. Xue *et al.*, "Extended equal area criterion revisited," *IEEE Trans. Power Syst.*, vol. 7, no. 3, pp. 1012–1022, Aug. 1992.

[3] M. Pavella, D. Ruiz-Vega, J. Giri, and R. Avila-Rosales, "An integrated scheme for on-line static and transient stability constrained ATC calculations," in *Proc. Power Eng. Soc. Summer Meeting*, vol. 1, Jul. 18–22, 1999, pp. 273–276.

[4] C. A. Canizares, "On bifurcations, voltage collapse and load modeling," *IEEE Trans. Power Syst.*, vol. 10, no. 1, pp. 512–522, Feb. 1995.

[5] H. D. Chiang, I. Dobson, R. J. Thomas, J. S. Thorp, and L. Fekih-Ahmed, "On voltage collapse in electric power systems," *IEEE Trans. Power Syst.*, vol. 5, no. 2, pp. 601–611, May 1990.

[6] T. Van Cutsem and C. D. Vournas, "Voltage stability analysis in transient and mid-term time scales," *IEEE Trans. Power Syst.*, vol. 11, no. 1, pp. 146–154, Feb. 1996.
[7] D. J. Hill and I. A. Hiskens, "Dynamic analysis of voltage collapse in power systems," in *Systems and Control Theory for Power Systems*, J. H. Chow, P. V. Kokotovic, and R. J. Thomas, Eds. New York: Springer-Verlag, 1995, pp. 157–172.
[8] I. A. Hiskens and D. J. Hill, "Incorporation of SVCs into energy function methods," *IEEE Trans. Power Syst.*, vol. 7, no. 1, pp. 133–140, Feb. 1992.
[9] R. J. Davy and I. A. Hiskens, "Lyapunov functions for multimachine power systems with dynamic loads," *IEEE Trans. Circuits Syst. I: Fundam. Theory Appl.*, vol. 44, no. 9, pp. 796–812, Sep. 1997.
[10] F. Howell and V. Venkatasubramanian, "Transient stability assessment with unstable limit cycle approximation," *IEEE Trans. Power Syst.*, vol. 14, no. 2, pp. 667–677, May 1999.
[11] H. Hashimoto, H. Taoka, M. Gibescu, and C.-C. Liu, "Energy-based evaluation of stability improvement by SVC with new second-kick design," *Trans. Inst. Elect. Eng. Jpn.*, vol. 122-B, no. 1, Jan. 2002.
[12] P. Kundur, *Power System Stability and Control*. New York: McGraw-Hill, 1993.
[13] K. Vu and C.-C. Liu, "Shrinking stability regions and voltage collapse in power systems," *IEEE Trans. Circuits Syst.*, vol. CAS-39, no. 4, pp. 271–289, Apr. 1992.
[14] T. J. Overbye, M. A. Pai, and P. W. Sauer, "Some aspects of the energy function approach to angle and voltage stability analysis in power systems," in *Proc. 31st Conf. Decision Control*, Tucson, AZ, Dec. 1992, pp. 2941–2946.
[15] N. Narasimhamurthi and M. T. Musavi, "A generalized energy function for transient stability analysis of power systems," *IEEE Trans. Circuits Syst.*, vol. CAS-31, no. 7, pp. 637–645, Jul. 1984.
[16] M. A. Pai, *Energy Function Analysis for Power System Stability*. Norwell, MA: Kluwer, 1989.
[17] C. K. Tang, C. E. Graham, M. El-Kady, and R. T. H. Alden, "Transient stability index from conventional time domain simulation," *IEEE Trans. Power Syst.*, vol. 9, no. 3, pp. 1524–1530, Aug. 1994.
[18] E. Vaahedi, Y. Mansour, A. Y. Chang, B. R. Corns, and E. K. Tse, "Enhanced second kick methods for on-line dynamic security assessment," *IEEE Trans. Power Syst.*, vol. 11, no. 4, pp. 1976–1982, Nov. 1996.
[19] H. D. Chiang and G. Cauley, "Direct stability analysis of electric power systems using energy functions: Theory, applications & perspective," *Proc. IEEE*, vol. 83, no. 11, pp. 1497–1529, Nov. 1995.
[20] A. C. Z. de Souza, C. A. Canizares, and V. H. Quintana, "New techniques to speed up voltage collapse computations using tangent vectors," *IEEE Trans. Power Syst.*, vol. 12, no. 3, pp. 1380–1387, Aug. 1997.
[21] P. Kundur, G. K. Morison, and L. Wang, "Techniques for on-line transient stability assessment and control," in *IEEE Power Eng. Soc. Winter Meeting*, vol. 1, Singapore, Jan. 2000, pp. 46–51.

Madeleine Gibescu (M'04) received the Dipl.Eng. degree in power engineering from the University of Politehnica, Bucharest, Romania, in 1993 and the M.S.E.E. and Ph.D. degrees from the University of Washington, Seattle, in 1995 and 2003, respectively.

She was a Power Systems Engineer for the AREVA T&D Corp. of Bellevue, WA. She is currently a visiting scholar with the Delft University of Technology, Delft, The Netherlands. Her research interests include power system dynamics and power system security in an open access environment.

Chen-Ching Liu (F'94) received the Ph.D. degree from the University of California, Berkeley, in 1983.

Since 1983, he has been on the faculty of the University of Washington, Seattle, where he is a Professor of Electrical Engineering and Associate Dean of Engineering. He is also the Director of the Electric Energy Industrial Consortium 1pand the Advanced Power Technologies Center at the University of Washington.

Dr. Liu was the recipient of the IEEE Millennium Medal in 2000.

Hiroyuki Hashimoto received the B.S. and M.S. degrees in electrical engineering from Kyoto University, Kyoto, Japan, in 1993 and 1995, respectively.

Since 1995, he has been with the Advanced Technology R&D Center, Mitsubishi Electric Corporation, Amagasaki, Japan. At present, his research interests include dynamic security assessment, generation scheduling, and risk assessment in the new deregulated power systems.

Mr. Hashimoto is a member of the Institute of Electrical Engineering of Japan.

Hisao Taoka (SM'97) received the B.S., M.S., and Ph.D. degrees from Tokyo University, Tokyo, Japan, in 1977, 1979, and 1986, respectively.

In 1979, he joined Mitsubishi Electric Corporation, Amagasaki, Japan, where he engaged in research on power system analysis and control. Since 2003, he has been with the Fukui University of Technology, Fukui, Japan, where he is a Professor of Electric and Electronics Engineering.

Dr. Taoka is a member of the Institute of Electrical Engineers of Japan and the CIGRE.